Deep learning-based brain age prediction in normal aging and dementia

Jeyeon Lee

Mayo Clinic

Brian Burkett

Mayo Clinic

Hoon-Ki Min

Mayo Clinic

Matthew Senjem

Mayo Clinic   https://orcid.org/0000-0001-9308-9275

Emily Lundt

Mayo Clinic

Hugo Botha

Mayo Clinic

Jonathan Graff-Radford

Mayo Clinic

Leland Barnard

Mayo Clinic

Jeffrey Gunter

Mayo Clinic

Christopher Schwarz

Mayo Clinic   https://orcid.org/0000-0002-1466-8357

Kejal Kantarci

Mayo Clinic

David Knopman

Mayo Clinic

Bradley Boeve

Mayo Clinic

Val Lowe

Mayo Clinic

Ronald Petersen

Mayo Clinic

Clifford Jack

Mayo Clinic Hospital   https://orcid.org/0000-0001-7916-622X

David Jones (Jones.david@mayo.edu)

---

1   **Deep learning-based brain age prediction in normal aging and dementia**

2

3   Jeyeon Lee[1], Brian J. Burkett[1], Hoon-Ki Min[1], Matthew L. Senjem[2], Emily S. Lundt[3], Hugo

4   Botha[4], Jonathan Graff-Radford[4], Leland R. Barnard[4], Jeffrey L. Gunter[1], Christopher G.

5   Schwarz[1], Kejal Kantarci[1], David S. Knopman[4], Bradley F. Boeve[4], Val J. Lowe[1], Ronald

6   C. Petersen[4], Clifford R. Jack Jr.[1], David T. Jones[4]*

7

8   [1] Department of Radiology, Mayo Clinic, Rochester, MN, USA

9   [2] Department of Information Technology, Mayo Clinic, Rochester, MN, USA

10   [3] Department of Health Sciences Research, Mayo Clinic, Rochester, MN, USA

11   [4] Department of Neurology, Mayo Clinic, Rochester, MN, USA

12   *Correspondence to: David T. Jones M.D., Mayo Clinic, Department of Neurology, 200

13   First Street SW, Rochester, Minnesota, 55905, USA

14   E-mail: Jones.david@mayo.edu

15

16   **Keywords:** Deep learning; Convolutional neural network; Brain age; Brain age gap;

17   Structural MRI; FDG PET; Saliency map; Dementia; Alzheimer's disease.

18

19   **Abstract**

20   Normal brain aging is accompanied by patterns of functional and structural change.

21   Alzheimer's disease (AD), a representative neurodegenerative disease, has been linked

22   to accelerated brain aging at respective age ranges. Here, we developed a deep

23   learning-based brain age prediction model using fluorodeoxyglucose (FDG) PET and

24 structural MRI and tested how the brain age gap relates to degenerative cognitive

25 syndromes including mild cognitive impairment, AD, frontotemporal dementia, and Lewy

26 body dementia. Occlusion analysis, performed to facilitate interpretation of the model,

27 revealed that the model learns an age- and modality-specific pattern of brain aging. The

28 elevated brain age gap in dementia cohorts was highly correlated with the cognitive

29 impairment and AD biomarker. However, regions generating brain age gaps were

30 different for each diagnosis group of which the AD continuum showed similar patterns to

31 normal aging in the CU.

32

33 **Introduction**

34 The biology of aging is complex[1] and has yet to be fully understood.[2] In general, aging

35 is characterized by the gradual accumulation of deleterious biological changes

36 accompanying a progressive loss of function[1], although this is not an all-encompassing

37 definition. The endeavor to better understand the biology of the aging brain is widely

38 relevant as the impact of aging on the human brain and associated changes in cognitive

39 function have implications for quality of life in the elderly.

40

41 The aging of the brain entails both structural and functional changes. Structural

42 magnetic resonance imaging (MRI) has shown that increased age is associated with

43 reduction of grey matter volume, most prominently in the frontal lobes, insular cortex,

44 and hippocampus[3-6], increased volume of the ventricular system and intracranial

45 cerebrospinal fluid[3,4,7], and changes in white matter microstructure.[7,8] In addition,

46 functional imaging techniques using positron emission tomography (PET) have shown

47   that brain aging is associated with decreased global oxygen utilization, cerebral blood

48   flow, glucose uptake, and regional changes in aerobic glycolysis.[9,10] Age-related

49   decreased glucose utilization has been found most prominently in the frontal lobes,

50   posterior cingulate, and posterior parietal lobes.[11-13] The temporal lobe, including medial

51   temporal regions - a critical area of pathology in dementia - has also showed an age-

52   dependent decrease in glucose metabolism.[14-16] In contrast, the primary motor cortex,

53   occipital cortex, cerebellum and sub-cortical structures including thalamus, putamen,

54   and pallidum have been found to be less susceptible to metabolic changes with aging.[17]

55

56   Based on these findings, age prediction using brain imaging is an active area of

57   neuroscience research.[18-22] An estimated age can be referred to as "brain age" for an

58   individual which may differ from the individual's chronological age.[19] Recently, growth in

59   data availability and advancement of deep learning (DL) techniques have allowed more

60   accurate brain-age estimation in the cognitively normal population through convolutional

61   neural network (CNN) models.[21-25] In addition, the 'brain age gap', which is the

62   difference between the 'predicted brain age' and 'chronological age', has been found to

63   be useful as a promising, personalized biomarker of brain health.[19] On an individual

64   basis, brain age gap measurements may also prove to have prognostic value,

65   potentially predicting health outcomes by capturing individual differences in the

66   interaction of aging and disease.[19] Several studies have reported that an over-

67   estimation of an individual's chronologic age based on a prediction from neuroimaging,

68   measured as a large brain age gap, is associated with mortality[26], neurodegenerative

69   diseases[27] and various other clinical conditions.[19,20] Moreover, measuring the brain age

70   gap in cases of neurodegenerative pathology may inform our understanding of disease

71   risk, resilience to structural/functional insults which accumulate with aging, and the

72   effects of diseases on the aging brain. For example, Alzheimer's disease has been

73   linked to accelerated brain aging at respective age ranges[28,29], implying that dementia is

74   an extreme phenotype of the aging process. Thus, a reliable measure of typical brain

75   aging may be beneficial in order to better distinguish from pathological aging.[30]

76

77   We aimed to develop a deep-learning-based brain age prediction model using a large

78   collection of brain structural MRI and Fluorodeoxyglucose (FDG) PET scans from

79   participants 20-98 years old (n = 2,349 unique individuals with 4,127 brain scans;

80   cognitively unimpaired (CU) normal controls =1,805 and cognitively impaired = 732).

81   Our brain age prediction method was developed using the images from only the CU

82   participants to train the healthy aging trajectories. We also studied age- and modality-

83   specific saliency maps of the CNN model explaining which brain regions contribute most

84   to age prediction for each age subgroup and modality type using an occlusion sensitivity

85   analysis. We then investigated the brain age gap estimation in the patient groups

86   including mild cognitive impairment (MCI), Alzheimer's disease (AD), Frontotemporal

87   Dementia (FTD), and Dementia with Lewy Bodies (DLB). We evaluated for associations

88   of brain age gap with neuropsychological tests and other imaging AD biomarkers, such

89   as amyloid PET and tau PET. We then performed a voxel-wise linear regression

90   analysis to look at which regional alterations contribute to higher brain age gap

91   generation for each disease group and compared them with normal brain aging

92   trajectories.

4

93

Results

Brain age estimation in CU participants. Our brain age prediction model based on
FDG PET or MRI was trained on CU participants in the Mayo dataset (n = 1,805) using
a 3D Densenet architecture (Fig. 1A).[31] For the training, we only utilized scans of the
first time point per a participant to avoid possible data leakage between the training and
validation/test sets. Then, the models were applied for predicting the brain age and the
accuracies were evaluated as a mean absolute error (MAE) with 5-fold cross validation.
Fig. 2 illustrates the scatterplots of the test set predictions against chronological age.
The result showed that our FDG- and MRI-based model could accurately predict the
chronological age of healthy adults (R^2 = 0.8546 and beta = 0.8503 for FDG and R^2 =
0.8046 and beta = 0.7718 for MRI). The overall performance measured on the test set
was MAE = 3.4333 ± 0.0545 and 4.2055 ± 0.2241 for FDG and MRI, respectively
(Supplementary table 2). As shown in Fig. 2b and e illustrating the scatterplot of brain
age gap (predicted brain age-chronological age) as a function of corresponding
chronological age, the estimation results showed a tendency to be biased towards the
mean age of the total cohort, resulting in a negative correlation between the brain age
gap and chronological age (*Spearman's r* = -0.3613 and -0.4642 for FDG and MRI,
respectively). This phenomenon is well-known to be associated with regression dilution
[32], model regularization and a non-Gaussian age distribution.[33] We used a linear bias
correction method[33] for age bias correction for the brain age gap. After the bias
correction, we observed that the correlation between the corrected brain age gap and
chronological age decreased to 0.0396 and 0.0303 for FDG and MRI respectively, and

116   MAE also decreased to 3.1212 and 3.3669 for FDG and MRI (Fig. 2c and f). The overall

117   performance after bias correction for total fold was MAE = 3.0755 ± 0.1401 and 3.4868

118   ± 0.1631 for FDG and MRI, respectively (Supplementary table 2).

119   To assess whether the trained model presents a dataset-specific bias, the model trained

120   with Mayo dataset was applied to an independent cohort, the Alzheimer's Disease

121   Neuroimaging initiative (ADNI; adni.loni.usc.edu) dataset (CU, n = 454). We obtained a

122   comparable result (corrected test MAE = 2.8942 for FDG and corrected test MAE =

123   3.5766 for MRI), implying that the models were fairly generalizable to the independent

124   dataset (Supplementary Fig. 1 and supplementary table 2). In addition, we also trained

125   a model by blending Mayo and ADNI dataset together (Supplementary Fig. 2). In this

126   trial, the overall performance of age prediction was better than using Mayo dataset only

127   (corrected test MAE = 2.7383 ± 0.1091 for FDG and corrected test MAE = 3.1029 ±

128   0.2107 for MRI; supplementary table 2).

129   To examine how the data-split option considering inter-participant variability and within-

130   participant variability affects performance, the prediction accuracies of several data-split

131   strategies were compared (as detailed in the methods section; Supplementary table 3).

132   Expectedly, we observed that the overlap of participants between the training dataset

133   and validation or test set significantly affected the accuracy of age estimation (option 2

134   and option 3 in supplementary table 3). This pattern was similarly found in both FDG

135   and MRI. On the other hand, whether to include multiple time points for each participant

136   has minimal effects on the model's performance (option 4 and option 5 in

137   supplementary table 3).

138

139   **Age- and modality-specific saliency map of brain age prediction model.** For an

140   interpretability of trained 3D-Densenet model, the saliency maps for age subgroups

141   were estimated through occlusion sensitivity analysis. In the occlusion sensitivity

142   analysis method, a portion of brain in the input space was occluded with a mask

143   (11x11x11) by setting these voxels to zero, and their relevance in the decisions was

144   indirectly estimated by calculating the change of MAE ($MAE_{occlusion}$ - $MAE_{original}$; Fig. 1B).

145   The results revealed age- and modality-specific saliency patterns (Fig. 3 and

146   supplementary Fig. 3). For the FDG model (left panel in Fig. 3), a posterior to anterior

147   transition was observed with increased age. The overall posterior region with a peak at

148   the posterior cingulate cortex had a higher contribution for age prediction in the younger

149   group (30-40 and 40-50 years). Meanwhile, for the 50-60 and 70-80 years of age

150   groups, the inferior frontal regions including the orbitofrontal and olfactory cortex were

151   dominantly utilized for age prediction. Prefrontal regions also showed a higher

152   contribution than other areas. A global contribution with the peak around the inferior

153   frontal cortex and basal ganglia was also found to be important for age prediction in the

154   older group (80-90 and 90-100 years). For MRI (right panel in Fig. 3), the insular cortex

155   contributed most to age prediction in the younger group (30-40 and 40-50 years). From

156   50-60 years, the ventricular boundary showed a higher contribution. The

157   cerebellomedullary cistern showed the highest saliency in the older groups (80-90 and

158   90-100 years).

159

160   **Brain age gap estimation in patient groups.** The brain age gap of four clinical

161   diagnosis groups (MCI, AD, FTD, and DLB) was estimated using the 3D-Densenet

162   model trained with normative cohorts. Fig. 4 illustrates the scatterplot of brain age gap

163   against chronological age for each patient group. The brain age gap was corrected

164   using the same coefficients used for bias correction of CU (Fig. 2). As expected, the

165   brain age gap of all patient groups was significantly higher than that of CU group for

166   both modalities ($P < 0.001$ two-sample t-test, Fig. 4e, and j). Interestingly, the predicted

167   brain age gap of all disease groups had a negative correlation with chronological age,

168   meaning younger patients had a higher gap. Accordingly, the mean brain age gap of

169   FTD, in which most patient was early onset, was relatively higher than that of other

170   groups, followed by AD, DLB, and MCI (Fig. 4e and j).

171   As shown in supplementary Fig. 4, FDG-based and MRI-based brain age gap showed

172   significant correlation with each other ($P < 0.001$, Pearson's correlation, Supplementary

173   Fig. 4) in every diagnostic group. Interestingly, the disease group tended to have a

174   higher correlation and slope than the CU cohort (Pearson's correlation: 0.5819, 0.7163,

175   0.7974, 0.8491 and 0.6925 for CU, MCI, AD, FTD and DLB, respectively, slope of fitted

176   line: 0.6624, 0.7080, 0.8102, 0.8132 and 0.8126 for CU, MCI, AD, FTD and DLB,

177   respectively).

178

179   **An association of brain age gap in dementia with normal aging.** Then, a voxel-wise

180   linear regression analysis was performed using the brain age gap as a regressor to

181   investigate which brain regions' alteration were related to higher brain age gap

182   generation for each patient group. In this analysis, chronological age was specified as a

183   nuisance covariate because it was negatively correlated with the brain age gap. As

184   illustrated in Fig. 5, FDG and MRI-based brain age gap showed different patterns

185   according to their disease group and imaging modality (using linear regression, FDR

186   corrected, $q < 0.01$, Fig. 5). In FDG, MCI and AD groups showed a negative correlation

187   throughout the brain, meaning global hypometabolism was associated with a higher

188   brain age gap (left panel in Fig. 5). In the AD group, the frontal, temporal, and parietal

189   regions showed a stronger negative correlation. In contrast, significant hypometabolism

190   related to the brain age gap was observed in the frontal and temporal regions in the

191   FTD patient group. Interestingly, the occipital cortex showed a positive correlation with

192   brain age gap in the FTD group. The DLB group showed a significant negative

193   correlation in posterior and temporal regions.

194   However, MRI showed a distinctly different pattern of salient regions from FDG (right

195   panel in Fig. 5). In MCI and AD, sulci and white matter showed a positive correlation,

196   and regions around the gyri and ventricles showed a negative correlation with brain age

197   gap. In contrast, a local negative correlation around the ventricles was marginally

198   observed for the FTD and DLB patient groups. To compare the observed brain age gap-

199   related changes with normal aging, a linear regression analysis was also performed for

200   the CU group using chronological age as a regressor (bottom row in Fig. 5). Similar to

201   the results for MCI and AD, a global negative correlation was observed on FDG PET. A

202   positive correlation in sulci and white matter and a negative correlation in areas around

203   the gyri and ventricles was observed on MRI. The voxel-wise correlation analysis

204   showed that the beta map of MCI and AD were more strongly correlated with that of

205   normal aging than FTD and DLB for FDG (Pearson's correlation; 0.9389, 0.8384,

206   0.6772 and 0.7239 for MCI, AD, FTD and DLB, respectively) and MRI (Pearson's

207 correlation; 0.8002, 0.7338, 0.4922 and 0.5356 for MCI, AD, FTD and DLB,

208 respectively).

209

210 **An association of brain age gap with neuropsychological test scores and AD**

211 **biomarkers.** As mentioned above, the high brain age gap has been found to be linked

212 to high cognitive impairments.[19,20,25] In light of this, the association was tested on the

213 corrected brain age gap of disease groups with the three cognitive test scores, including

214 Clinical Dementia Rating sum of boxes (CDR-SB)[34], Short Test of Mental Status

215 (STMS)[35], and Mini-Mental State Examinations (MMSE)[36]. As expected, both FDG-

216 based and MRI-based brain age gap showed significant correlations with the three

217 scores ($P < 0.001$, Pearson's correlation, Fig. 6).

218 Then, we sought to examine an association of brain age gap with neuroimaging

219 biomarkers for AD. AD is characterized by a pathology aggregation of beta-amyloid (Aβ)

220 and neurofibrillary tangles which can be captured by Pittsburgh Compound B (PiB) PET

221 and tau PET respectively. PiB and tau PET quantification was performed on meta-ROI

222 that has previously been shown to have a broad dynamic range across the normal to

223 pathological aging to AD dementia. A meta-ROI PiB PET standardized uptake value

224 ratio (SUVr) was derived from the average of the median SUVr in the prefrontal,

225 orbitofrontal, parietal, temporal, anterior cingulate, and posterior cingulate/precuneus

226 regions.[37] A meta-ROI tau PET SUVr was formed from the average of the median

227 uptake in the amygdala, entorhinal cortex, fusiform, parahippocampal and inferior

228 temporal and middle temporal gyri.[37] For meta-ROI PiB PET SUVr, only the MCI group

229 reached statistical significance. In FDG and MRI, the correlation coefficient was

230   marginal and there was no obvious pattern of association in distribution (Fig. 7a and e).

231   Other disease groups did not show significance (Fig. 7b-d and f-h). However, meta-ROI

232   tau PET SUVr showed a significant correlation with brain age gap in the MCI and AD

233   groups (Fig. 7i-j and m-n). In particular, the AD group showed a higher correlation

234   (r=0.5110 for FDG and r=0.6648 for MRI, Fig. 7j and n). FTD and DLB patients showed

235   no significant correlation with meta-ROI tau PET SUVr.

236

237   **Discussion**

238   We developed a 3D DenseNet model, trained on structural and metabolic brain images,

239   that generates an accurate estimate of an individual's brain age during normal cognitive

240   aging. An occlusion analysis revealed anatomic regions critical to the model

241   performance and demonstrated an age-dependent saliency pattern of brain regions.

242   The patterns were distinct for each input imaging modality, structural MRI vs. FDG PET,

243   which is interesting given that the predictive accuracy of the FDG and MRI models were

244   similar. In cohorts with a neurological disorder, the brain age gap was larger than

245   cognitively CU individuals and significantly correlated with the cognitive score. Anatomic

246   regions with the greatest weight in generating the brain age gap, identified from the

247   voxel-wise linear regression analysis, were different for each diagnostic group. The

248   results for the AD continuum, MCI and AD, showed close correlation to normal aging

249   compared to FTD or DLB, with an accelerated time frame in the MCI and AD groups

250   reflected by the larger brain age gap compared to normal aging.

251   Most previous brain age studies were based on structural MRI.[21-26,38] To our knowledge,

252   only one prior study utilized FDG PET[18], but that study was based on a non-DL method

253 and utilized a substantially smaller cohort size (n=205). The structural and functional

254 changes contributing to precise age prediction in the DL approach remain to be fully

255 elucidated. One of the major limitations of studies using a CNN is the interpretability of

256 the model. A limited number of structural MRI-based studies reported explanation maps

257 of the CNN model.[21,22,24] Although CNN-based age prediction has provided high

258 accuracy, it is difficult to know which features are important for age estimation.

259 Furthermore, there is a dearth of knowledge regarding which brain alterations and

260 specific regional changes are associated with higher brain age gaps in patients.

261

262 Brain-specific prediction of age is of interest both as a component of overall biologic age

263 assessment, but also as a biomarker for age-associated neurologic diseases and

264 changes in neurologic function. In a broad sense, age prediction may help to elucidate

265 the relationship of the aging process to degenerative pathology. Is dementia a

266 consequence of a unique pathologic mechanism or instead an accelerated version of

267 normal aging?[39] If dementia reflects a continuum of the underlying changes in brain

268 structure and metabolism to which all individuals are inevitably susceptible at various

269 rates, brain age-prediction based on neuroimaging may yield a better understanding of

270 different metabolic brain aging phenotypes. Alternatively, if types of dementia represent

271 entities with distinctly different mechanisms than normal aging, markers of brain age

272 may still prove useful in identifying individuals at greater risk for developing these

273 conditions.[39,40]

274

275   Our model was able to precisely estimate an individual's chronological age based on

276   structural and metabolic neuroimaging data (corrected MAE = 3.0755 ± 0.1401 and

277   3.4868 ± 0.1631 for FDG PET and MRI, respectively). Interestingly, FDG-based brain

278   age prediction was slightly better than the MRI-based model (Fig. 2 and supplementary

279   table 2), implying that metabolic data may be more sensitive for tracking normal brain

280   aging trajectories. One consideration is that metabolic changes detectable on PET may

281   precede structural changes observed in AD[41], although this has not been characterized

282   in CU. Also, our FDG PET model did partially incorporate structural information since

283   the spatial normalization to template space for the FDG PET scan was performed using

284   the subject's MR images, meaning the brain-age prediction model using FDG PET has

285   the benefit of both functional and structural information. FDG PET images are also

286   affected by structural changes via partial volume effects. Alternatively, the improved

287   performance of the model using PET relative to MRI could be a consequence of

288   regional heterogeneity in age-related structural changes in the brain.[42]

289   Occlusion analysis shows a distinct age-specific saliency pattern according to input

290   imaging modality (Fig. 3 and supplementary Fig. 3). In the FDG-based model, a

291   transition of posterior to anterior structures with increased age was observed. The

292   posterior structures, especially the posterior cingulate cortex (PCC), contributed most in

293   younger age groups, whereas anterior structures including the frontotemporal lobes

294   were more critical in older age groups. The high contribution of PCC is consistent with

295   previously described FDG PET study demonstrating a significant correlation of glucose

296   metabolism decline in the PCC with age.[11] Interestingly, amyloid deposition and

297   reduced glucose metabolism in the PCC has been implicated in early AD.[43] In older

13

298   adults, FDG activity in frontal regions with a peak around inferior frontal and

299   orbitofrontal, and also global activity were found to contribute the most to age prediction.

300   The decline of frontal metabolism in normal aging was consistently reported across

301   several studies.[14,44] The orbitofrontal cortex is also a known region of prominent age-

302   related hypometabolism on PET.[44]

303

304   On the other hand, the MRI based model's saliency map demonstrated different critical

305   regions compared to the FDG PET analysis. For younger age groups, the insula was

306   identified as the most critical region. The insula has been identified as a region of gray

307   matter volume loss with normal aging.[45] Additionally, the medial temporal lobe

308   structures were identified as areas with high saliency in the MRIs of younger, 30-50

309   year old individuals, regions of previously described volume loss with aging as well as

310   AD.[46] Preservation of brain parenchyma in the insula and medial temporal lobe of

311   younger individuals may have been a reliable feature for MRI-based age-prediction. For

312   older age groups, the cerebellomedullary cistern and the peripheral boundaries of the

313   ventricles were critical. This may reflect reliance of the age-prediction model on the

314   typical enlargement of the CSF spaces which occurs with age.[3,4,7] Age-dependent

315   enlargement of the ventricles is an established phenomenon, though varies in

316   individuals.[47] Interestingly, saliency maps did not show a prominent contribution of

317   cortical regions for age estimation, which we expected to find due to the typical age-

318   dependent decrease in cortical volume seen on MRI.[45,47] We speculate that cortical

319   volume loss with age may be too heterogenous to serve as the most-reliable salient

320   feature for the age-prediction model. Change in white matter signal characteristics is

321   also a well-known phenomenon of aging.[48] No contribution of white matter was found

322   with our occlusion analysis, which might be a consequence of white matter intensity

323   normalization performed on the MRI exams.

324   Consistent with previous findings, the estimated brain age gap of neurodegenerative

325   disease groups was larger than the CU group and significantly correlated with cognitive

326   scores. Interestingly, the estimated brain age gap is negatively correlated with

327   chronologic age for both MRI and FDG (Fig. 4) and was close to zero in older age

328   groups. This implies that normal elderly brain is indistinguishable from the diseased

329   brain at a similar older age with the DenseNet model. The brain age gap of MCI and AD

330   showed a significant association with tau PET, but not amyloid PET using PiB (Fig. 7).

331   Tau is well known to be more closely related to the AD severity than PiB.[49] In both

332   preclinical AD and AD dementia, tau radiotracer uptake and cortical thickness have

333   been found to correlate with decreased cognitive task performance to a greater degree

334   than amyloid beta radiotracer uptake.[49] However, the relationship between aging and

335   AD is complex. It has been suggested that on closer examination, differences in rates of

336   cognitive decline, structural changes, and clinical features point toward AD as a discrete

337   entity that cannot be simply described as accelerated aging process.[40]

338   A strong correlation was shown between FDG- and MRI-based brain age gap in the CU

339   cohort and also in the neurodegenerative disease groups (supplementary Fig. 3). This

340   result implies that the metabolic changes of normal aging, as well as disease

341   progression, are concurrent with the structural changes, with respect to factors that

342   impact the performance of the age-prediction model. The correlation between FDG- and

343   MRI-based brain age gap is mildly stronger in disease groups ($r = 0.6925$ to 0.8491)

344   than in the CU cohort (*r* = 0.5819). The structural changing or atrophy in

345   neurodegenerative pathology accompanying hypometabolism, to a greater extent than

346   with normal aging, is one plausible explanation for the increased correlation in diseased

347   groups. Alternatively, brain FDG hypometabolism, which occurs in specific patterns for

348   different categories of neurodegenerative pathology[50], may correlate more closely with

349   structural or volumetric changes for specific neurodegenerative disease cohorts than in

350   normal aging.

351   In FTD, frontal and anterior temporal regions showed a negative correlation with brain

352   age gap, regions with characteristic hypometabolism in FTD[51,52]; and a positive

353   correlation was observed in the occipital lobe, a region typically without hypometabolism

354   on FDG PET in FTD.[51,52] Castelnova et al also reported that some FTD cases showed

355   occipital hypermetabolism.[53] In DLB, temporal, parietal and occipital regions were

356   negatively correlated with brain age gap, regions of hypometabolism frequently

357   observed in DLB.[51] Correlation of the occipital lobe and primary visual cortex in the DLB

358   group is notable because occipital/primary visual cortex hypometabolism is

359   characteristic of DLB on FDG PET from other neurodegenerative processes such as

360   AD.[51,54] The ability of the FDG metabolic signature to distinguish DLB from AD is unique

361   and an important component of the clinical utility of FDG PET[55], as abnormal amyloid

362   beta PET which is a defining hallmark of AD, is commonly present in DLB due to the

363   phenomenon of co-occurring pathologies with advancing age.[54] The ventricle and

364   boundaries of brain parenchyma with CSF space were correlated with MCI and AD in

365   MRI. For FTD and DLB, the ventricular boundary was correlated with brain age gap,

366   although no correlation was seen at the CSF and cortical region. Periventricular borders

367   with CSF may reflect areas of white matter volume loss and the gyral/sulcal interface

368   may reflect, which both also occur with normal aging.[3,4,7]

369   This study has some notable limitations. In the occlusion analysis, left hemispheric

370   dominance was observed in the contribution to brain age prediction, which was not

371   explainable by post-hoc analysis. The occlusion-based method has been described to

372   focus more on the most dominant regions compared to other interpretation methods.[56]

373   In this study, we only tested neurodegenerative pathology, without evaluating any

374   chronic systemic medical diseases and vascular diseases which may have different

375   patterns of brain aging, a limitation of this study.

376

377   In summary, we showed that 3D-DenseNet brain age prediction model generates

378   accurate age prediction for CU individuals, with slightly more robust performance using

379   an FDG PET input than MRI. Brain age prediction using PET imaging input, which

380   reflects metabolic function, may present a distinct assessment of brain health from the

381   structural information evaluated on MRI. The brain age gap from MRI or PET data is

382   increased in multiple types of dementia compared to CU individuals and therefore may

383   prove to be a useful composite biomarker to identify increased risk for pathology or

384   marker of disease severity.

385   **Materials and methods**

386   **Dataset.** A large number of participants (Table 1) ranging in age from 20 to 98 years old

387   were included (n = 2,349, number of scans = 4,127) who had both MRI and FDG PET

388   from the Mayo Clinic Study of Aging (MCSA) or the Alzheimer's Disease Research

389   Center (ADRC) study (Table 1). All participants or designees provided written consent

390   with the approval of Mayo Clinic and Olmsted Medical Center Institutional Review

391   Boards. As previously described, the Mayo Clinic Rochester ADRC is a longitudinal

392   cohort study that enrolls participants from the clinical practice at Mayo Clinic in

393   Rochester, MN.[57] The MCSA is a population-based study of cognitive aging among

394   Olmsted County, MN residents.[58] Enrolled participants are adjudicated to be clinically

395   normal or cognitively impaired by a consensus panel consisting of study coordinators,

396   neuropsychologists and behavioral neurologists. Methods for defining clinically

397   unimpaired, mild cognitive impairment and dementia in both of these studies conform to

398   standards in the field.[59-61] For this analysis, the participants were assigned into six

399   clinical sub-groups based on clinical diagnosis following consensus criteria[54,62] including

400   CU (n = 1,805, number of scans = 2,879), MCI (n = 480, number of scans = 666), AD (n

401   = 215, number of scans = 372), FTD (n = 45, number of scans = 69) and DLB (n = 86,

402   number of scans = 141).

403   For the CNN model training, only CU data was utilized. Some participants also

404   underwent amyloid PET scanning with PiB (number of scans=2,508) and tau PET scans

405   with flortaucipir (number of scans=608). Most participants had CDR-SB[34], STMS[35], and

406   MMSE[36] available (n = 2,511, 2,511 and 2,464, respectively). All cognitive tests were

407   administered by experienced psychometrists and supervised by board-certified clinical

408   neuropsychologists. To examine whether the trained model presents a dataset-specific

409   bias, we also utilized ADNI dataset (n = 1,150, number of scans = 1,622; supplementary

410   table 1). The ADNI dataset included CU (n = 330, number of scans = 454), MCI (n=647,

411   number of scans = 885) and dementia (n = 255, number of scans = 283).

412

413   **Image processing.** T1-weighted MRI scans were acquired using 3T scanners. FDG

414   PET imaging was performed with ^{18}F-FDG, amyloid PET with PiB[63] and tau PET with

415   Flortaucipir (AV-1451).[64] FDG PET images were acquired from 30-40 minutes, PiB PET

416   from 40-60 minutes, and tau PET from 80-100 minutes after injection. CT was obtained

417   for attenuation correction. PET images were analyzed with our in-house fully automated

418   image processing pipeline.[65] Briefly, the PET scans were co-registered to the

419   corresponding MRI for each participant within each timepoint, and subsequently warped

420   to Mayo Clinic Adult Lifespan Template (MCALT) space[66]

421   (https://www.nitrc.org/projects/mcalt/) using the warps from SPM12 Unified

422   Segmentation.[67] The corresponding MRI was corrected for intensity inhomogeneity and

423   segmented using MCALT tissue priors and segmentation parameters. FDG PET SUVr

424   was calculated by dividing the median of uptake in pons and the SUVr images were

425   used for input data to the CNN model. Amyloid and tau PET SUVr were calculated by

426   dividing the median uptake in the cerebellar crus grey matter.[37] A meta-ROI PiB PET

427   SUVr was derived from the average of the median SUVr in the prefrontal, orbitofrontal,

428   parietal, temporal, anterior cingulate, and posterior cingulate/precuneus regions.[37] A

429   meta-ROI tau PET SUVr was formed from the average of the median uptake in the

430   amygdala, entorhinal cortex, fusiform, parahippocampal and inferior temporal and

431   middle temporal gyri.[37] For each MRI volume, voxels' intensities were normalized by

432   dividing a mean intensity derived from individualized white matter mask.[68]

433

434   **3D-Densenet architecture and training.** A modified 3D-Densenet model[31] was trained

435   on FDG PET or MRI scans of cognitively unimpaired cohort (Fig. 1A). For the training,

436   we only utilized scans of the first time point (n = 1,805) to avoid data leakage between

437   the training and validation/test sets. Experimental tests measuring how an overlap of

438   participants among training, validation and test sets affected the model's results were

439   performed separately (see Dataset split experiment section). A schematic of the 3D-

440   DenseNet architecture is shown in Fig 1A. The specific dimension of input data was

441   121x145x121, in our applications. The output to be predicted was a single scalar

442   representing the chronological age (years). The architecture was comprised of a regular

443   3 × 3 × 3 convolutional layer followed by four dense blocks and three transition blocks in

444   between them. The four dense blocks consisted of 3, 6, 12, and 8 dense layers,

445   respectively (denoted above each block). Each dense layer had a 1 × 1 × 1 bottleneck

446   convolutional layer followed by a 3 × 3 × 3 convolution layer. The dense layers were

447   densely interconnected in a feed-forward manner within each block. The growth rate (k)

448   was 48. The flattened output from the last global average pooling layer was then fully

449   connected with 1,457 units and was connected to the output layer.

450   The neural network was implemented using Keras with Tensorflow[69] as the backend.

451   Cross-validated experiments were conducted using 5-fold validations (60% training set,

452   20% validation set and 20% test set). Mean absolute error (MAE) was used as the loss

453   function. The model was optimized using the Adam optimizer with parameters: $\beta 1$=0:9

454   and $\beta 2$=0.99.[70] The He initialization strategy was used for the weight initialization.[71] The

455   training epoch was 150. The learning rate selected for the training set was 1×10^{-4} and

456   decreased by a factor of 2 for every ten epochs. If the validation error did not improve in

457   7 epochs, the learning rate was updated. The total number of parameters were

458   70,183,073, of which 70,122,657 were trainable parameters. We used a mini-batch size

459 of 4. Training and testing were performed on a Tesla P100 GPU. The source code is

460 available online (https://github.com/Neurology-AI-Program/Brain_age_prediction.git).

461

462 **Occlusion sensitivity analysis.** To facilitate interpretability, we generated brain maps

463 of the relevant features used in the age prediction model using occlusion sensitivity

464 analysis.[72] The analysis was conducted within the test set. To calculate the age-specific

465 saliency map, the data were separated into seven sub-age groups based on their

466 chronological age, from 30 to 100 with 10 years interval. Within each group, the original

467 images were occluded by 11x11x11 voxel areas with zero values, along a 11x11x11

468 grid (Fig. 1B). Since the front and rear 12 voxels along the anterior-posterior axes do

469 not include the brain area, those were excluded from occlusion to reduce the

470 computational load. Then, age inference on the occluded images was performed

471 through our pre-trained 3D Densenet model and the performance was evaluated as

472 $MAE_{occlusion}$. The delta MAE was obtained by calculating the difference between

473 $MAE_{occlusion}$ and $MAE_{original}$ acquired through the original image, and a delta MAE matrix

474 (11x11x11) was obtained by iterating occlusion for every region (n=1,331). Then, the

475 delta MAE matrix was reconstructed into the original image size (121x145x121) through

476 cubic interpolation and zero-padding for the excluded area in the occlusion, and the

477 average of the five folds was calculated. Normalization was performed by dividing the

478 entire image by the maximum value, and thus, the values of final saliency map ranged

479 from 0 to 1.

480

481   **Dataset split experiment.** To measure how the inclusion of multiple time points per

482   participant affects brain age prediction, we tested five different data split options. The

483   main result was derived from the strictest data split option: Option 1 using only a single

484   time point per participant. Four additional options were tested: Option 2 (multiple-time

485   points per participant with overlap between training, validation, and test sets permitted);

486   Option 3 (multiple-time points per participant with overlap between training and

487   validation sets permitted); Option 4 (multiple time points for the training and validation

488   sets and a single time point for the test set; no overlap of participants amongst training,

489   validation, and test sets were permitted); and Option 5 (a single time point was used for

490   the validation and test sets; no overlap of participants among training, validation, and

491   test sets). For these five options, the validation MAE and test MAE from five-fold cross-

492   validations were compared (Supplementary table 3).

493

494   **Statistical analysis.** The brain age prediction accuracy was assessed by MAE and

495   Spearman correlation between predicted age and chronological age. Defining x to be

496   chronological age and y the predicted age, the brain age gap was calculated by y - x.

497   The brain age gap is known to be correlated with chronological age, which results in an

498   overestimation for younger individuals and an underestimation for older individuals[21,38]

499   due to regression dilution.[32] Therefore, we used the linear bias correction method

500   described in[33] for age bias correction for the brain age gap. We fitted a linear regression

501    $y = a$x$ + b$ to the test set. Then, the corrected brain age gap was calculated by $(y-b)/a -$

502   x. The a and b coefficient derived from the CU group was applied to other diagnostic

503   groups in the same way for the bias correction. The corrected brain age gap of disease

504 groups was compared with CU by a two-sample t-test. The Pearson correlation

505 coefficient was utilized to test for an association between the corrected brain age gap

506 and cognitive scores. A voxel-wise regression analysis was performed using the brain

507 age gap as a regressor to investigate which brain regions' alteration was associated

508 with brain age gap generation for each patient group. Each individual's chronological

509 age was specified as nuisance covariance. For CU participants, the same analysis was

510 performed using chronological age as a regressor. Statistical significance was corrected

511 for multiple comparisons using a false discovery rate (FDR)[73] with a cluster size of at

512 least 100 adjacent voxels. An association of corrected brain age gap with meta-ROI PiB

513 PET SUVr and meta-ROI tau PET SUVr was assessed by Pearson correlation.

514

525

526 **Author contributions**

527 Conceptualization: J.L., HK. M., and D.T.J. Software: J.L. and L.R.B. Preprocessing:

528 M.L.S. Methodology: J.L., H.K.M., M.L.S., E.S.L., H.B., and C.G.S. Writing—original

529 draft: J.L., B.J.B., H.K.M., V.J.L. and D.T.J. Writing— revisions: All authors. Supervision:

530 V.J.L., C.R.J., and D.T.J. All authors have given final approval of this version of the

531 article.

532

533 **Competing interests**

534 The authors report no competing interests.

535

536 **References**

537 1   López-Otín, C., Blasco, M. A., Partridge, L., Serrano, M. & Kroemer, G. The hallmarks
538   of aging. *Cell* **153**, 1194-1217 (2013).
539 2   Harman, D. Aging: overview. *Annals of the New York Academy of Sciences* **928**, 1-21
540   (2001).
541 3   Courchesne, E. *et al.* Normal brain development and aging: quantitative analysis at in
542   vivo MR imaging in healthy volunteers. *Radiology* **216**, 672-682 (2000).
543 4   Good, C. D. *et al.* A voxel-based morphometric study of ageing in 465 normal adult
544   human brains. *Neuroimage* **14**, 21-36 (2001).
545 5   Sowell, E. R. *et al.* Mapping cortical change across the human life span. *Nature*
546   *neuroscience* **6**, 309-315 (2003).
547 6   Lemaitre, H. *et al.* Normal age-related brain morphometric changes: nonuniformity
548   across cortical thickness, surface area and gray matter volume? *Neurobiology of aging*
549   **33**, 617. e611-617. e619 (2012).
550 7   Raz, N. & Rodrigue, K. M. Differential aging of the brain: patterns, cognitive correlates
551   and modifiers. *Neuroscience & Biobehavioral Reviews* **30**, 730-748 (2006).
552 8   Walhovd, K. B. *et al.* Effects of age on volumes of cortex, white matter and subcortical
553   structures. *Neurobiology of aging* **26**, 1261-1270 (2005).
554 9   Goyal, M. S. *et al.* Loss of brain aerobic glycolysis in normal human aging. *Cell*
555   *metabolism* **26**, 353-360. e353 (2017).
556 10   Goyal, M. S., Hawrylycz, M., Miller, J. A., Snyder, A. Z. & Raichle, M. E. Aerobic
557   glycolysis in the human brain is associated with development and neotenous gene
558   expression. *Cell metabolism* **19**, 49-57 (2014).
559 11   Zuendorf, G., Kerrouche, N., Herholz, K. & Baron, J. C. Efficient principal component
560   analysis for multivariate 3D voxel-based mapping of brain functional imaging data sets as
561   applied to FDG-PET and normal aging. *Human brain mapping* **18**, 13-21 (2003).

562 12 Knopman, D. S. *et al.* 18F-fluorodeoxyglucose positron emission tomography, aging, and
563 apolipoprotein E genotype in cognitively normal persons. *Neurobiology of aging* **35**,
564 2096-2106 (2014).
565 13 De Leon, M. *et al.* Prediction of cognitive decline in normal elderly subjects with 2-[18F]
566 fluoro-2-deoxy-D-glucose/positron-emission tomography (FDG/PET). *Proceedings of the*
567 *National Academy of Sciences* **98**, 10966-10971 (2001).
568 14 De Santi, S. *et al.* Age-related changes in brain: II. Positron emission tomography of
569 frontal and temporal lobe glucose metabolism in normal subjects. *Psychiatric Quarterly*
570 **66**, 357-370 (1995).
571 15 Bonte, S. *et al.* Healthy brain ageing assessed with 18F-FDG PET and age-dependent
572 recovery factors after partial volume effect correction. *European journal of nuclear*
573 *medicine and molecular imaging* **44**, 838-849 (2017).
574 16 Shen, X., Liu, H., Hu, Z., Hu, H. & Shi, P. The relationship between cerebral glucose
575 metabolism and age: report of a large brain PET data set. *PloS one* **7**, e51517 (2012).
576 17 Petit-Taboue, M., Landeau, B., Desson, J., Desgranges, B. & Baron, J. Effects of healthy
577 aging on the regional cerebral metabolic rate of glucose assessed with statistical
578 parametric mapping. *Neuroimage* **7**, 176-184 (1998).
579 18 Goyal, M. S. *et al.* Persistent metabolic youth in the aging female brain. *Proceedings of*
580 *the National Academy of Sciences* **116**, 3251-3255 (2019).
581 19 Cole, J. H. & Franke, K. Predicting age using neuroimaging: innovative brain ageing
582 biomarkers. *Trends in neurosciences* **40**, 681-690 (2017).
583 20 Cole, J. H. Multimodality neuroimaging brain-age in UK biobank: relationship to
584 biomedical, lifestyle, and cognitive factors. *Neurobiology of aging* **92**, 34-42 (2020).
585 21 Bashyam, V. M. *et al.* MRI signatures of brain age and disease over the lifespan based on
586 a deep brain network and 14 468 individuals worldwide. *Brain* **143**, 2312-2324 (2020).
587 22 Abrol, A. *et al.* Deep learning encodes robust discriminative neuroimaging
588 representations to outperform standard machine learning. *Nature communications* **12**, 1-
589 17 (2021).
590 23 Cole, J. H. *et al.* Predicting brain age with deep learning from raw imaging data results in
591 a reliable and heritable biomarker. *NeuroImage* **163**, 115-124 (2017).
592 24 Levakov, G., Rosenthal, G., Shelef, I., Raviv, T. R. & Avidan, G. From a deep learning
593 model back to the brain—Identifying regional predictors and their relation to aging.
594 *Human brain mapping* **41**, 3235-3252 (2020).
595 25 Jónsson, B. A. *et al.* Brain age prediction using deep learning uncovers associated
596 sequence variants. *Nature communications* **10**, 1-10 (2019).
597 26 Cole, J. H. *et al.* Brain age predicts mortality. *Molecular psychiatry* **23**, 1385-1392
598 (2018).
599 27 Gaser, C. *et al.* BrainAGE in mild cognitive impaired patients: predicting the conversion
600 to Alzheimer's disease. *PloS one* **8**, e67346 (2013).
601 28 Habes, M. *et al.* Advanced brain aging: relationship with epidemiologic and genetic risk
602 factors, and overlap with Alzheimer disease atrophy patterns. *Translational psychiatry* **6**,
603 e775-e775 (2016).
604 29 Jones, D. T. *et al.* Age-related changes in the default mode network are more advanced in
605 Alzheimer disease. *Neurology* **77**, 1524-1531 (2011).

606 30 Lorenzi, M., Pennec, X., Frisoni, G. B., Ayache, N. & Initiative, A. s. D. N.
607   Disentangling normal aging from Alzheimer's disease in structural magnetic resonance
608   images. *Neurobiology of aging* **36**, S42-S52 (2015).
609 31 Huang, G., Liu, Z., Van Der Maaten, L. & Weinberger, K. Q. in *Proceedings of the IEEE*
610   *conference on computer vision and pattern recognition.* 4700-4708.
611 32 MacMahon, S. *et al.* Blood pressure, stroke, and coronary heart disease: part 1, prolonged
612   differences in blood pressure: prospective observational studies corrected for the
613   regression dilution bias. *The Lancet* **335**, 765-774 (1990).
614 33 Smith, S. M., Vidaurre, D., Alfaro-Almagro, F., Nichols, T. E. & Miller, K. L. Estimation
615   of brain age delta from brain imaging. *NeuroImage* **200**, 528-539 (2019).
616 34 Morris, J. C. Clinical dementia rating: a reliable and valid diagnostic and staging measure
617   for dementia of the Alzheimer type. *International psychogeriatrics* **9**, 173-176 (1997).
618 35 Kokmen, E., Smith, G. E., Petersen, R. C., Tangalos, E. & Ivnik, R. C. The short test of
619   mental status: correlations with standardized psychometric testing. *Archives of neurology*
620   **48**, 725-728 (1991).
621 36 Folstein, M. F., Folstein, S. E. & McHugh, P. R. "Mini-mental state": a practical method
622   for grading the cognitive state of patients for the clinician. *Journal of psychiatric*
623   *research* **12**, 189-198 (1975).
624 37 Jack Jr, C. R. *et al.* Defining imaging biomarker cut points for brain aging and
625   Alzheimer's disease. *Alzheimer's & Dementia* **13**, 205-216 (2017).
626 38 Peng, H., Gong, W., Beckmann, C. F., Vedaldi, A. & Smith, S. M. Accurate brain age
627   prediction with lightweight deep neural networks. *Medical image analysis* **68**, 101871
628   (2021).
629 39 Berg, L. Does Alzheimer's disease represent an exaggeration of normal aging? *Archives*
630   *of Neurology* **42**, 737-739 (1985).
631 40 Toepper, M. Dissociating normal aging from Alzheimer's disease: A view from cognitive
632   neuroscience. *Journal of Alzheimer's disease* **57**, 331-352 (2017).
633 41 Chételat, G. *et al.* Direct voxel-based comparison between grey matter hypometabolism
634   and atrophy in Alzheimer's disease. *Brain* **131**, 60-71 (2008).
635 42 Salat, D. H. *et al.* Thinning of the cerebral cortex in aging. *Cerebral cortex* **14**, 721-730
636   (2004).
637 43 Buckner, R. L. *et al.* Molecular, structural, and functional characterization of Alzheimer's
638   disease: evidence for a relationship between default activity, amyloid, and memory.
639   *Journal of neuroscience* **25**, 7709-7717 (2005).
640 44 Curiati, P. *et al.* Age-Related Metabolic Profiles in Cognitively Healthy Elders: Results
641   from a Voxel-Based [18F] Fluorodeoxyglucose–Positron-Emission Tomography Study
642   with Partial Volume Effects Correction. *American journal of neuroradiology* **32**, 560-565
643   (2011).
644 45 Long, X. *et al.* Healthy aging: an automatic analysis of global and regional morphological
645   alterations of human brain. *Academic radiology* **19**, 785-793 (2012).
646 46 Jack, C. R. *et al.* Rate of medial temporal lobe atrophy in typical aging and Alzheimer's
647   disease. *Neurology* **51**, 993-999 (1998).
648 47 Davis, P. C., Mirra, S. S. & Alazraki, N. The brain in older persons with and without
649   dementia: findings on MR, PET, and SPECT images. *AJR. American journal of*
650   *roentgenology* **162**, 1267-1278 (1994).

651 48 Habes, M. *et al.* White matter hyperintensities and imaging patterns of brain ageing in the
652 general population. *Brain* **139**, 1164-1179 (2016).
653 49 Ossenkoppele, R. *et al.* Associations between tau, Aβ, and cortical thickness with
654 cognition in Alzheimer disease. *Neurology* **92**, e601-e612 (2019).
655 50 Shivamurthy, V. K., Tahari, A. K., Marcus, C. & Subramaniam, R. M. Brain FDG PET
656 and the diagnosis of dementia. *American Journal of Roentgenology* **204**, W76-W85
657 (2015).
658 51 Brown, R. K., Bohnen, N. I., Wong, K. K., Minoshima, S. & Frey, K. A. Brain PET in
659 suspected dementia: patterns of altered FDG metabolism. *Radiographics* **34**, 684-701
660 (2014).
661 52 Kanda, T. *et al.* Comparison of grey matter and metabolic reductions in frontotemporal
662 dementia using FDG-PET and voxel-based morphometric MR studies. *European journal*
663 *of nuclear medicine and molecular imaging* **35**, 2227-2234 (2008).
664 53 Castelnovo, V. *et al.* Heterogeneous brain FDG-PET metabolic patterns in patients with
665 C9orf72 mutation. *Neurological Sciences* **40**, 515-521 (2019).
666 54 McKeith, I. G. *et al.* Diagnosis and management of dementia with Lewy bodies: Fourth
667 consensus report of the DLB Consortium. *Neurology* **89**, 88-100 (2017).
668 55 Graff-Radford, J. *et al.* 18F-fluorodeoxyglucose positron emission tomography in
669 dementia with Lewy bodies. *Brain communications* **2**, fcaa040 (2020).
670 56 Rieke, J., Eitel, F., Weygandt, M., Haynes, J.-D. & Ritter, K. in *Understanding and*
671 *Interpreting Machine Learning in Medical Image Computing Applications* 24-31
672 (Springer, 2018).
673 57 Jones, D. T. *et al.* Tau, amyloid, and cascading network failure across the Alzheimer's
674 disease spectrum. *Cortex* **97**, 143-159 (2017).
675 58 Roberts, R. O. *et al.* The Mayo Clinic Study of Aging: design and sampling,
676 participation, baseline measures and sample characteristics. *Neuroepidemiology* **30**, 58-
677 69 (2008).
678 59 Albert, M. S. *et al.* The diagnosis of mild cognitive impairment due to Alzheimer's
679 disease: recommendations from the National Institute on Aging-Alzheimer's Association
680 workgroups on diagnostic guidelines for Alzheimer's disease. *Alzheimer's & dementia* **7**,
681 270-279 (2011).
682 60 McKhann, G. M. *et al.* The diagnosis of dementia due to Alzheimer's disease:
683 recommendations from the National Institute on Aging-Alzheimer's Association
684 workgroups on diagnostic guidelines for Alzheimer's disease. *Alzheimer's & dementia* **7**,
685 263-269 (2011).
686 61 Petersen, R. C. Mild cognitive impairment as a diagnostic entity. *Journal of internal*
687 *medicine* **256**, 183-194 (2004).
688 62 Neary, D. *et al.* Frontotemporal lobar degeneration: a consensus on clinical diagnostic
689 criteria. *Neurology* **51**, 1546-1554 (1998).
690 63 Klunk, W. E. *et al.* Imaging brain amyloid in Alzheimer's disease with Pittsburgh
691 Compound-B. *Annals of Neurology: Official Journal of the American Neurological*
692 *Association and the Child Neurology Society* **55**, 306-319 (2004).
693 64 Xia, C. F. *et al.* [18F] T807, a novel tau positron emission tomography imaging agent for
694 Alzheimer's disease. *Alzheimer's & Dementia* **9**, 666-676 (2013).

695 65 Schwarz, C. G. *et al.* A comparison of partial volume correction techniques for
696   measuring change in serial amyloid PET SUVR. *Journal of Alzheimer's Disease* **67**, 181-
697   195 (2019).
698 66 Schwarz, C. *et al.* in *Alzheimer's Association International Conference.[Google*
699   *Scholar].*
700 67 Ashburner, J. & Friston, K. J. Unified segmentation. *Neuroimage* **26**, 839-851 (2005).
701 68 Shinohara, R. T. *et al.* Statistical normalization techniques for magnetic resonance
702   imaging. *NeuroImage: Clinical* **6**, 9-19 (2014).
703 69 Abadi, M. *et al.* in *12th {USENIX} symposium on operating systems design and*
704   *implementation ({OSDI} 16).* 265-283.
705 70 Kingma, D. P. & Ba, J. Adam: A method for stochastic optimization. *arXiv preprint*
706   *arXiv:1412.6980* (2014).
707 71 He, K., Zhang, X., Ren, S. & Sun, J. in *Proceedings of the IEEE international conference*
708   *on computer vision.* 1026-1034.
709 72 Zeiler, M. D. & Fergus, R. in *European conference on computer vision.* 818-833
710   (Springer).
711 73 Genovese, C. R., Lazar, N. A. & Nichols, T. Thresholding of statistical maps in
712   functional neuroimaging using the false discovery rate. *Neuroimage* **15**, 870-878 (2002).
713

714

Figures and Tables.

Figure1. 3D Densenet architecture for age prediction and layout of occlusion
analysis.
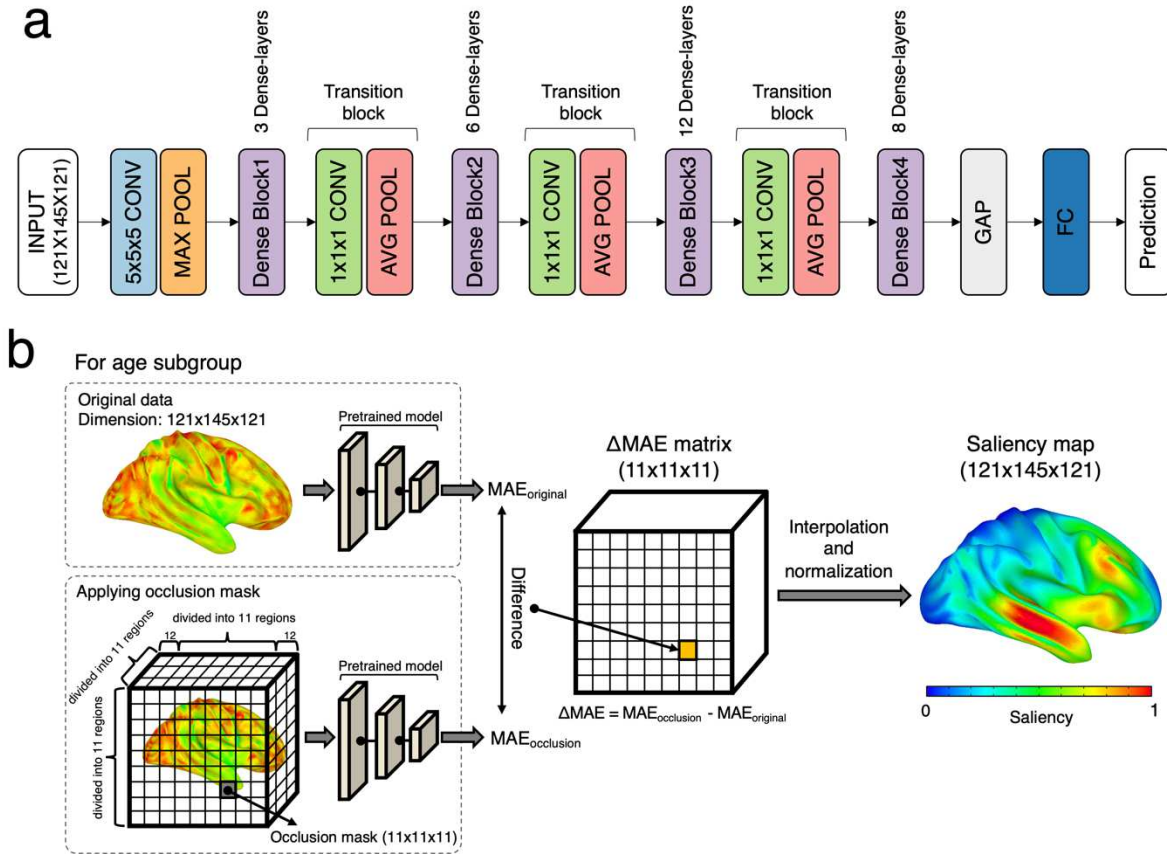
Figure1. 3D Densenet architecture for age prediction and layout of occlusion

analysis. a, The detailed architecture of the 3D Densenet used for age prediction.

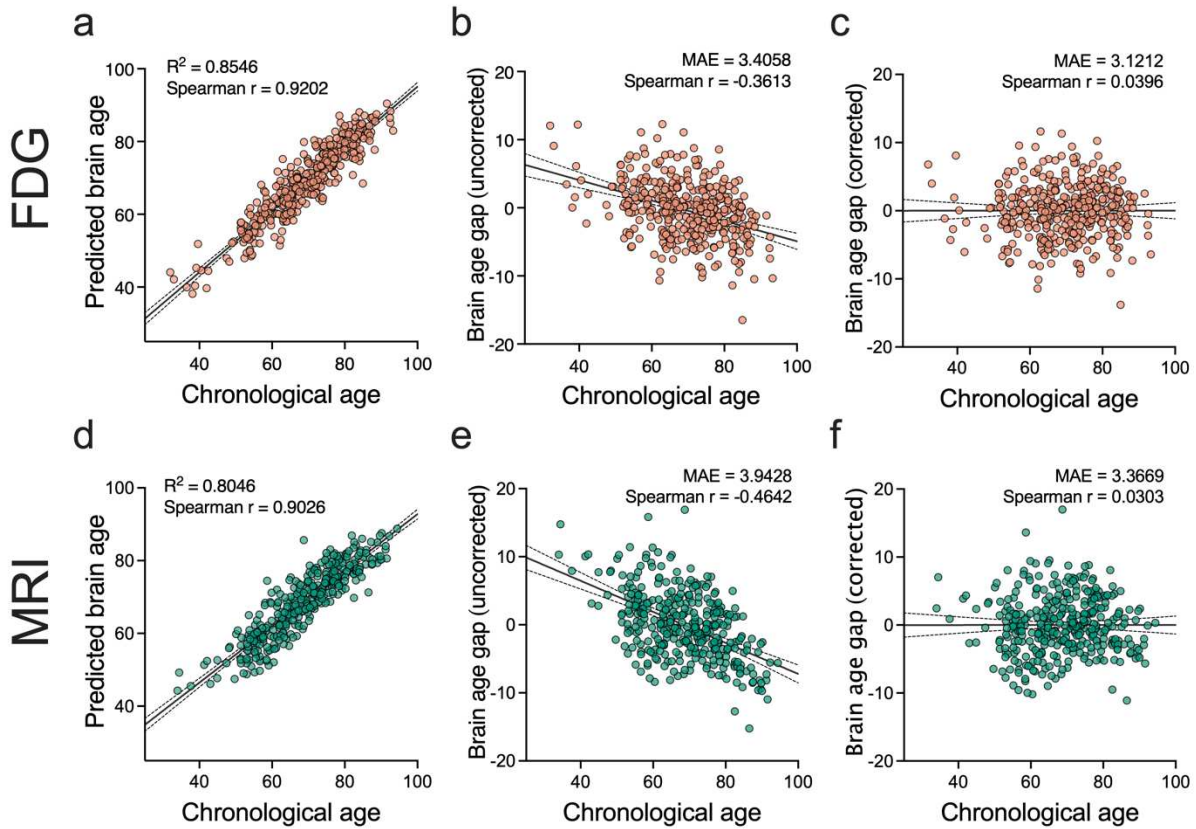CONV = convolutional layer, MAX POOL = max pooling layer, AVG POOL = average

pooling layer, GAP = global average pooling layer, FC = fully connected layer. **b,**

Illustration of the framework for occlusion analysis.

Figure 2. Brain age predictions on CU participants.

Figure 2. Brain age predictions on CU participants. (a-c) FDG based brain age

prediction result for the test set of the representative fold. **a,** A regression plot showing

chronological age vs. predicted brain age. **b,** The uncorrected brain age gap. **c,** The

brain age gap after bias correction. **(d-f)** MRI-based brain age prediction result for the

test set of the representative fold. **d,** A regression plot showing chronological age vs.

predicted brain age. **e,** The uncorrected brain age gap. **f,** The brain age gap after bias

correction. The black solid line and dotted lines in each figure represent a regression

line and its 95% confidence bands, respectively.

739 **Figure 3. The visualization of model activation shown on coronal slices.**
740
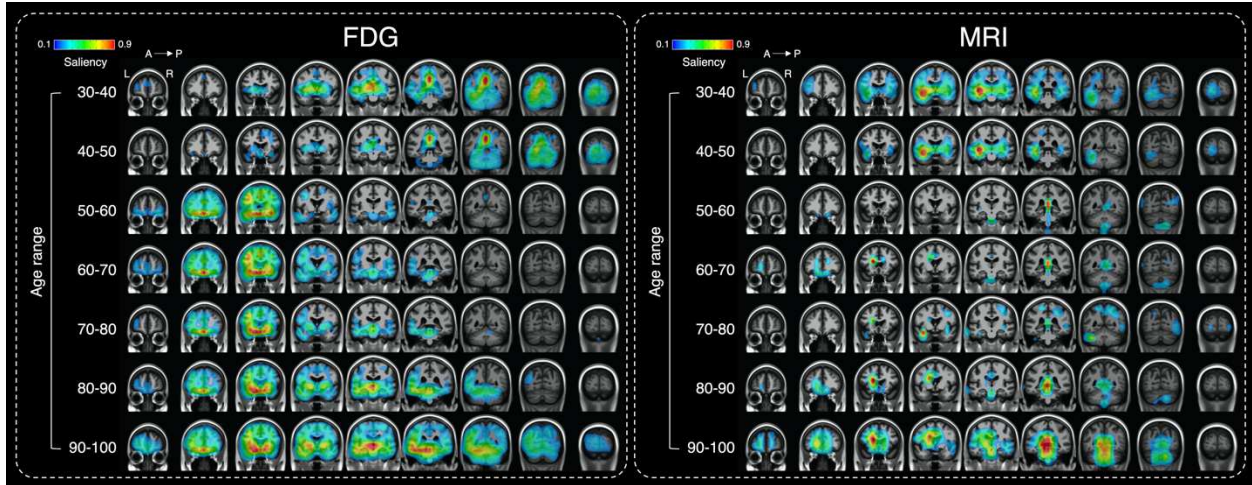
741
742
743 **Figure 3. The visualization of model activation shown on coronal slices.** Saliency

744 maps were computed using occlusion sensitivity analysis for each age range group.

745 Higher activation represents the importance of a region in brain age estimation. A left

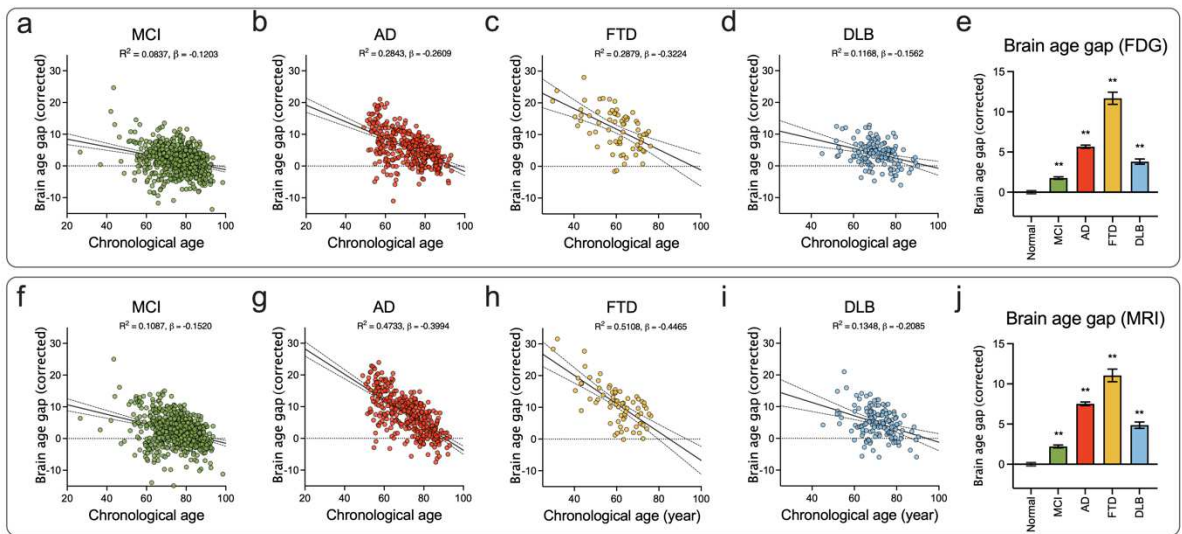746 panel shows the saliency maps for the FDG-based model and a right panel shows the

747 saliency maps for MRI-based model.

748
749

Figure 4. Regression plots of a corrected brain age gap as a function of chronological age for clinical diagnostic groups.

Figure 4. Regression plots of a corrected brain age gap as a function of chronological age for clinical diagnostic groups. (a-d) FDG-based brain age gap estimation for MCI, AD, FTD and DLB, respectively. **e,** Mean of corrected brain age gap for each diagnostic group. Error bars indicate the standard error of the mean. ** $p < 0.001$ comparison with CU, two-sample t-test. **(f-i)** MRI-based brain age gap estimation for MCI, AD, FTD and DLB, respectively. **j,** Mean of corrected brain age gap for each clinical diagnosis group. Error bars indicate the standard error of the mean. ** $p < 0.001$ comparison with CU, two-sample t-test.

Figure 5. Voxel-wise linear regression analysis of brain age gap.
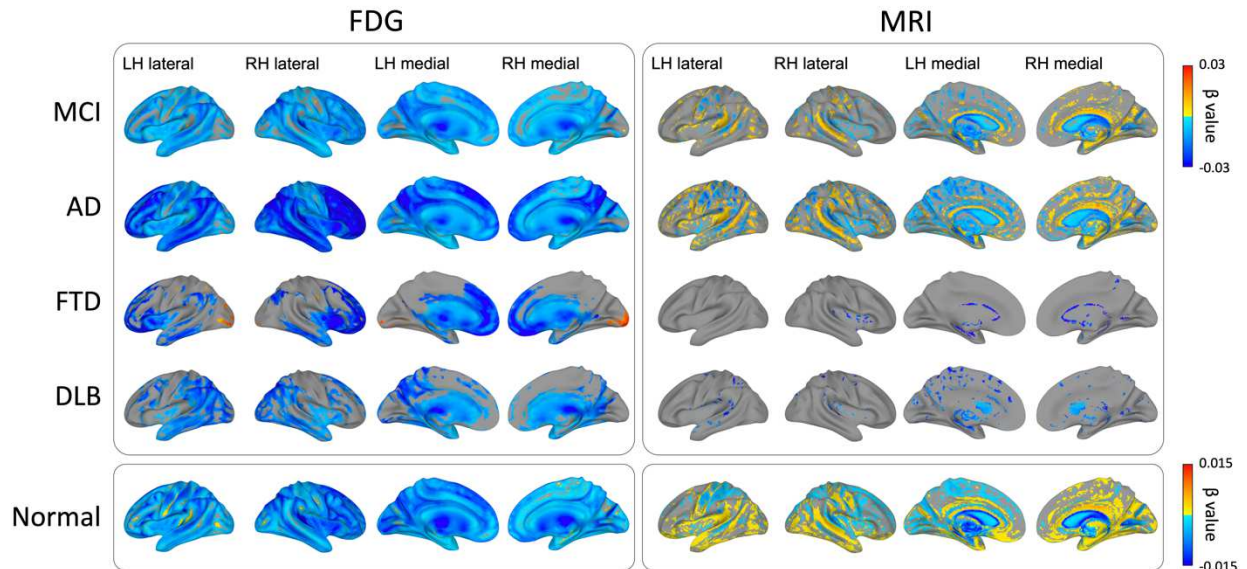
Figure 5. Voxel-wise linear regression analysis of brain age gap. Clinical diagnosis

group (MCI, AD, FTD and DLB)-specific results from voxel-wise whole-brain linear

regression examining the brain age gap-related change (FDR corrected, q<0.01). The

chronological age was specified as nuisance covariance. For CU (bottom row), voxel-

wise linear regression analysis was performed using the chronological age as a

regressor to show the age-related change. A left panel shows the results for the FDG-

based model and a right panel shows the results for the MRI-based model.
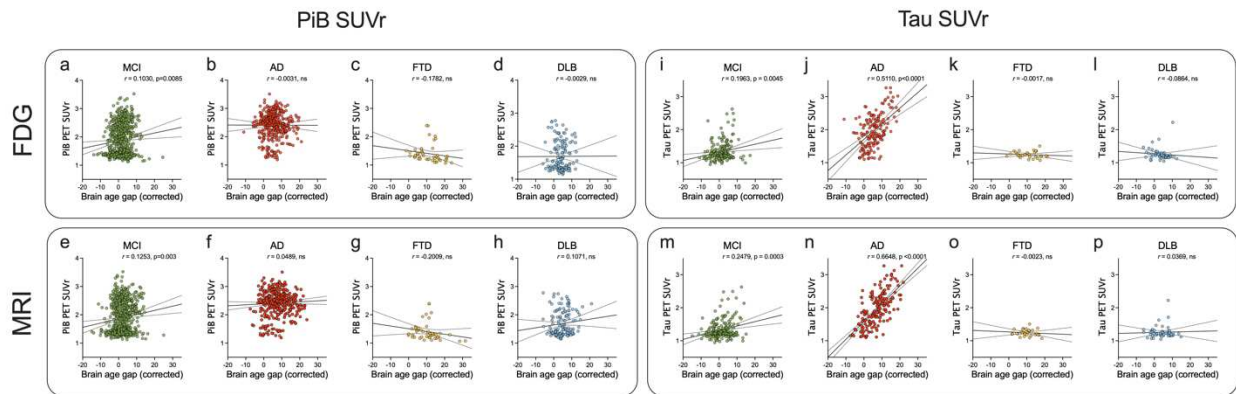
Figure 6. Association of a brain age gap with cognitive scores.
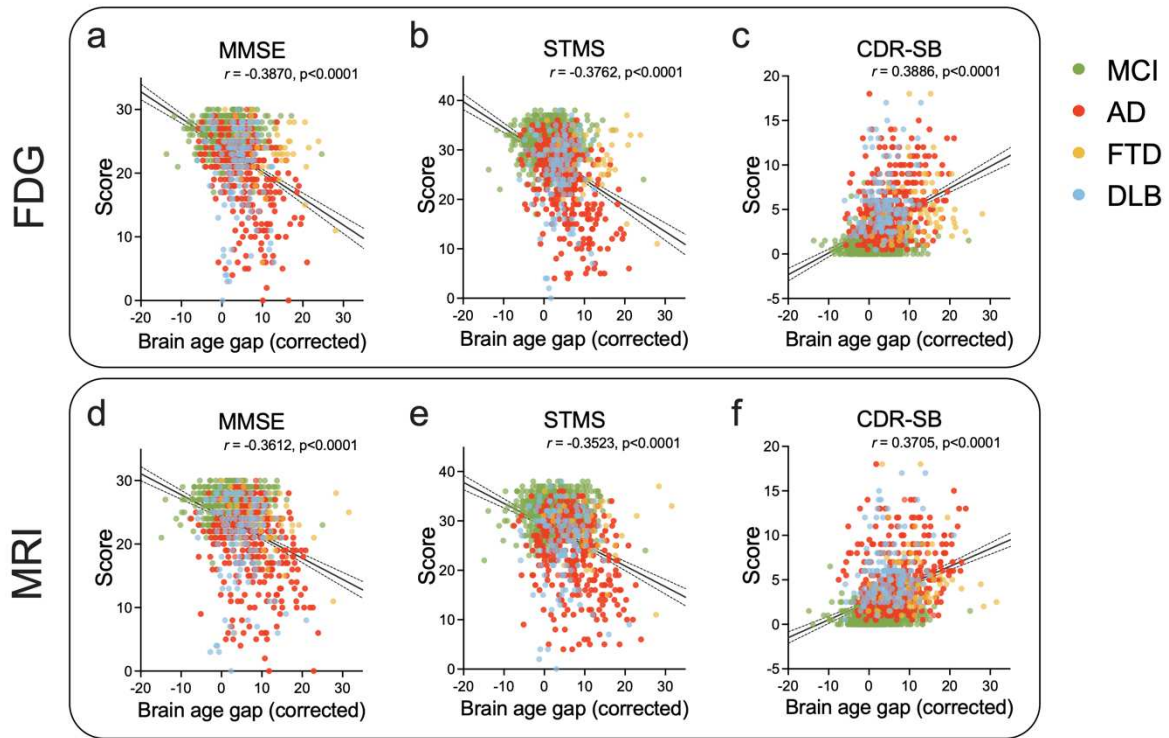
776
777 **Figure 6. Association of a brain age gap with cognitive scores. (a-c)** Scatter plots

778 of FDG model-based brain age gap with Mini-Mental State Examinations (MMSE), Short

779 Test of Mental Status (STMS) and Clinical Dementia Rating Sum of boxes (CDR-SB),

780 respectively. **(d-f)** Scatter plots of MRI model-based brain age gap with MMSE, STMS

781 and CDR-SB, respectively.

782

Figure 7. Association of brain age gap with meta-ROI PiB- and Tau PET SUVr.

Figure 7. Association of brain age gap with meta-ROI PiB- and Tau PET SUVr. (a-d) Scatter plots show the relationship between FDG-based brain age gap with meta-ROI PiB PET SUVr for MCI, AD, FTD and DLB, respectively. **(e-h)** Scatter plots show the relationship between MRI-based brain age gap with meta-ROI PiB SUVr for MCI, AD, FTD and DLB, respectively. **(i-l)** Scatter plots show the relationship between FDG-based brain age gap with meta-ROI Tau PET SUVr for MCI, AD, FTD and DLB, respectively. **(m-p)** Scatter plots show the relationship between MRI-based brain age gap with meta-ROI Tau PET SUVr for MCI, AD, FTD and DLB, respectively. The black solid line and dotted lines in each figure represent a regression line and its 95% confidence bands, respectively. r indicates Pearson's correlation coefficient.

35

**Table 1. Demographics of Mayo dataset**

Characteristic	Clinical Diagnosis				
	Normal	MCI	AD	FTD	DLB
N	1,805	480	215	45	86
Total time points, n (%)					
1	973 (53.91)	190 (39.58)	80 (37.21)	19 (42.22)	44 (51.16)
2	503 (27.87)	130 (27.08)	72 (33.49)	10 (22.22)	15 (17.44)
3	243 (13.46)	86 (17.92)	31 (14.42)	8 (17.78)	10 (11.63)
4+	86 (4.76)	74 (15.42)	32 (14.88)	8 (17.78)	17 (19.76)
Age, years					
Median (IQR)	72 (62 79)	77 (70 83)	74 (64 79.75)	63 (55 70.25)	71 (66 77)
Min Max	30 97	26 98	49 92	31 76	45 90
Male sex, n (%)	952 (52.74)	319 (66.46)	117 (54.42)	26 (57.78)	74 (86.05)
Education, years, median (IQR)	15 (13 17)	14 (12 16)	16 (12 17.75)	16 (13 17.25)	15.5 (13 18)
Clinical Dementia Rating Scale-Sum of Boxes, median (IQR)	0 (0 0)	0.5 (0.5 0.5)	1 (0.5 1)	1 (0.5 1)	1 (0.5 1)
Mini-Mental State Examinations, median (IQR)	29 (28 29)	27 (24 28)	21 (17 24)	24 (21 26)	23 (17 25.25)
Short Test of Mental Status, median (IQR)	36 (34 37)	32 (29 34)	25 (19 29)	28 (25 31.5)	27 (22 30)

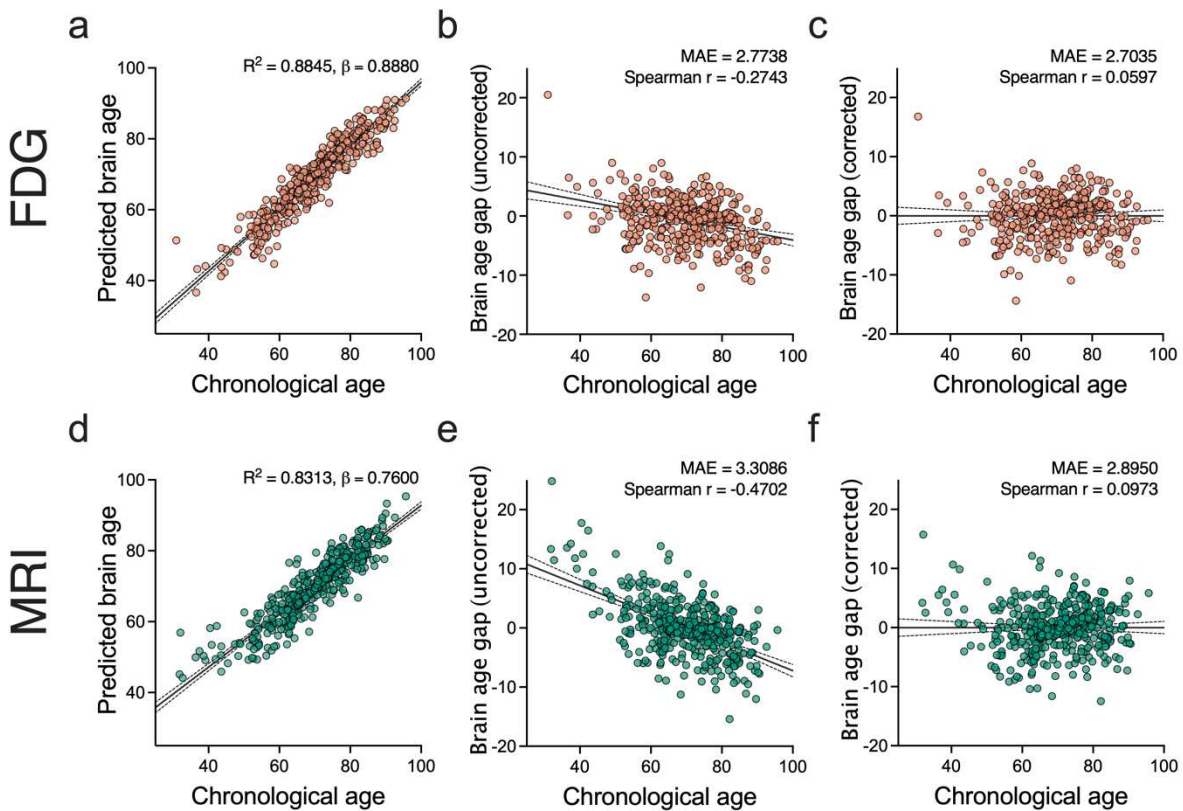801 **Supplementary figure 1. Brain age predictions on the ADNI dataset.**
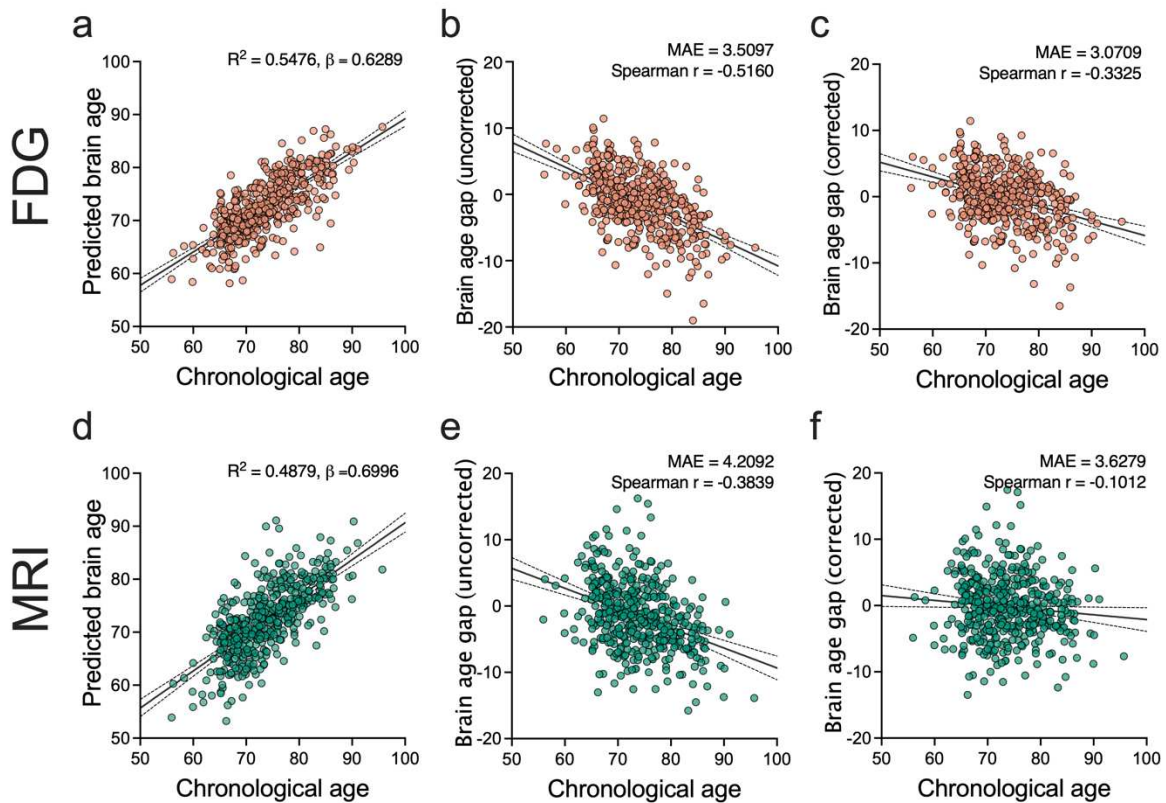
802
803
804 **Supplementary figure 1. Brain age predictions on the ADNI dataset.** 3D Densenet

805 model trained on the Mayo dataset was applied to the ADNI data. **(a-c)** FDG based

806 brain age prediction result for the test set. **a,** A regression plot showing chronological

807 age vs. predicted brain age. **b,** The uncorrected brain age gap. **c,** The brain age gap

808 after bias correction. **(d-f)** MRI-based brain age prediction result for the test set. **d,** A

809 regression plot showing chronological age vs. predicted brain age. **e,** The uncorrected

810 brain age gap. **f,** The brain age gap after bias correction. The black solid line and dotted

811 lines in each figure represent a regression line and its 95% confidence bands,

812 respectively.

813
814

**Supplementary figure 2. Brain age predictions on the Mayo + ADNI dataset.**

Prediction performance of 3D Densenet model trained on the Mayo and ADNI dataset together. **(a-c)** FDG based brain age prediction result for the test set. **a,** A regression plot showing chronological age vs. predicted brain age. **b,** The uncorrected brain age gap. **c,** The brain age gap after bias correction. **(d-f)** MRI-based brain age prediction result for the test set. **d,** A regression plot showing chronological age vs. predicted brain age. **e,** The uncorrected brain age gap. **f,** The brain age gap after bias correction. The black solid line and dotted lines in each figure represent a regression line and its 95% confidence bands, respectively.

Supplementary figure 3. Regional mean saliency.
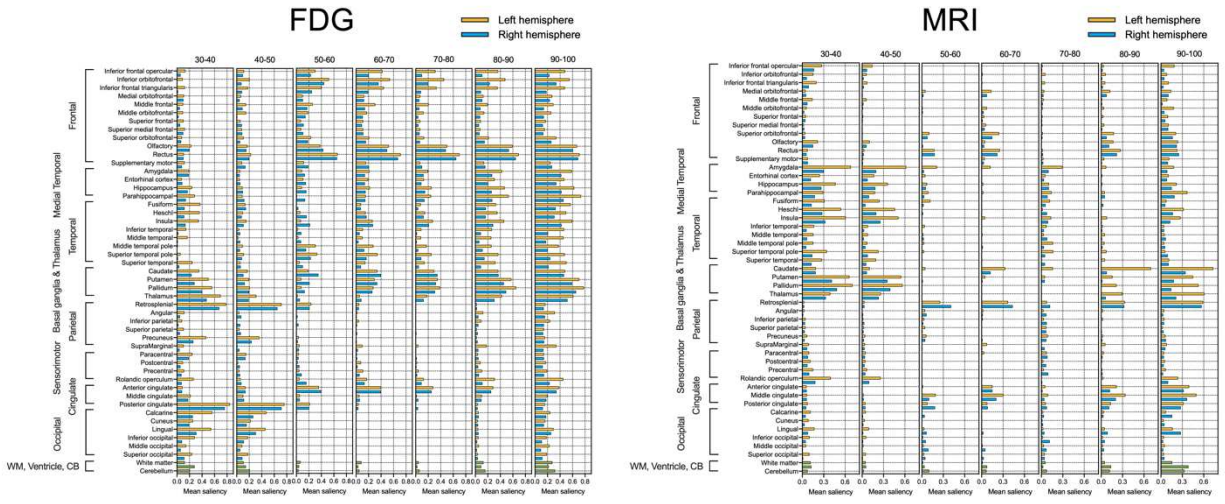
829
830
831 **Supplementary figure 3. Regional mean saliency.** After calculating the saliency map

832 from occlusion analysis, mean saliency value was calculated for each ROI. Yellow-

833 colored bars indicate the left hemisphere and blue-colored bars indicate the right

834 hemisphere.

835

836 **Supplementary figure 4. Relationship between FDG- and MRI-based brain age**
837 **gap.**
838
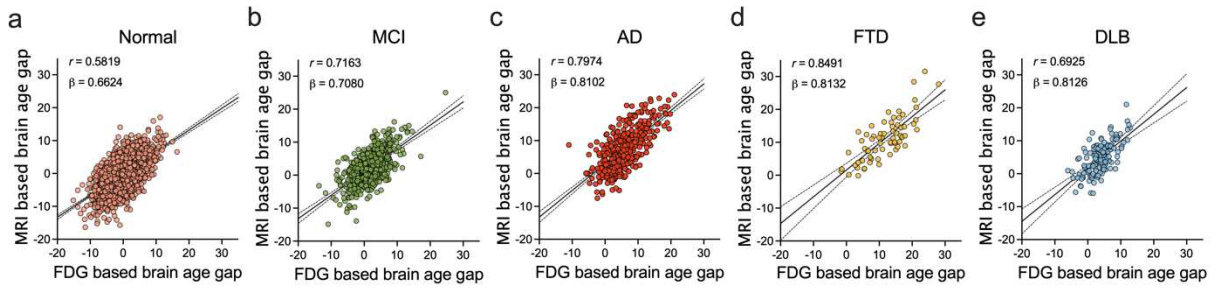
839
840

841 **Supplementary figure 4. Relationship between FDG- and MRI-based brain age**

842 **gap. a,** CU. **b,** MCI. **c,** AD. **d,** FTD. **e,** DLB. The black solid line and dotted lines in each

843 figure represent a regression line and its 95% confidence bands, respectively. *r*

844 indicates Pearson's correlation coefficient.

845
846

847 **Supplementary table 1. Demographics of ADNI dataset.**

Characteristic	Clinical Diagnosis		
	Normal	MCI	AD
N	330	647	255
Total time points, n (%)			
1	208 (63.03)	443 (68.47)	227 (89.02)
2	120 (36.36)	170 (26.28)	28 (10.98)
3	2 (0.61)	34 (5.26)	
Age, years			
Median (IQR)	73 (69 78)	74 (68 79)	76 (71 81)
Min Max	56 96	55 94	56 96
Male sex, n (%)	152 (46.06)	356 (55.02)	145 (56.86)
Education, years, median (IQR)	16 (15 18)	16 (14 18)	16 (14 18)

848

849

850 **Supplementary table 2. Summary table of model performance.**

Modality	Dataset	Val. MAE (yrs)	Uncorrected test MAE (yrs)	Corrected test MAE (yrs)
FDG	Mayo	3.4558 ± 0.1121	3.4333 ± 0.0545	3.0755 ± 0.1401
	Mayo model to ADNI		3.5097	2.8942
	Mayo + ADNI	3.0450 ± 0.1360	2.9943 ± 0.1472	2.7383 ± 0.1091
MRI	Mayo	4.1438 ± 0.2012	4.2055 ± 0.2241	3.4868 ± 0.1631
	Mayo model to ADNI		4.2092	3.5766
	Mayo + ADNI	3.4886 ± 0.1764	3.5712 ± 0.2010	3.1029 ± 0.2107

851

852

853   **Supplementary table 3. Data split strategy comparison**

Modality	Strategy	Val. MAE (yrs)	Uncorrected Test MAE (yrs)	Corrected Test MAE (yrs)
FDG	Option 1	3.4558 ± 0.1121	3.4333 ± 0.0545	3.0755 ± 0.1401
	Option 2	2.8381 ± 0.0820	2.8161 ± 0.0581	2.5773 ± 0.0791
	Option 3	2.7197 ± 0.0609	3.2983 ± 0.1221	3.0606 ± 0.1489
	Option 4	3.3894 ± 0.1209	3.3853 ± 0.1339	3.0609 ± 0.1388
	Option 5	3.4094 ± 0.0977	3.4227 ± 0.1717	3.0822 ± 0.1515
MRI	Option 1	4.1438 ± 0.2012	4.2055 ± 0.2241	3.4868 ± 0.1631
	Option 2	3.4013 ± 0.0789	3.4101 ± 0.0556	2.9606 ± 0.1152
	Option 3	3.1033 ± 0.1384	3.8923 ± 0.1896	3.3339 ± 0.0870
	Option 4	3.9168 ± 0.1332	4.0508 ± 0.1326	3.4393 ± 0.1612
	Option 5	4.0204 ± 0.1145	4.0417 ± 0.0999	3.4701 ± 0.1333

854

855

856   **Supplementary table 4. Association of brain age gap with cognitive scores.**

Modality	Cognitive test	Brain age gap correlation	95% CI	P Value	R^2
	MMSE	-0.3870	-0.4289 to -0.3434	<0.0001	0.1498
FDG	Kokmen Short test	-0.3762	-0.4190 to -0.3318	<0.0001	0.1415
	CDR sum of box	0.3886	0.3460 to 0.4296	<0.0001	0.1510
	MMSE	-0.3612	-0.4041 to -0.3167	<0.0001	0.1305
MRI	Kokmen Short test	-0.3523	-0.3960 to -0.3070	<0.0001	0.1241
	CDR sum of box	0.3705	0.3272 to 0.4122	<0.0001	0.1373

857
858